# Novel Designs for Thermally Robust Coplanar Crossing in QCA

Sanjukta Bhanja
Electrical Engineering Department
University of South Florida, Tampa, FL
bhanja@eng.usf.edu

Marco Ottavi, Fabrizio Lombardi
Electrical & Computer Engineering Department
Northeastern University
Boston, MA
{mottavi,lombardi}@ece.neu.edu

Salvatore Pontarelli
Dipartimento di Ingegneria Elettronica
Università di Roma "Tor Vergata"
Rome, ITALY
pontarelli@ing.uniroma2.it

## Abstract

*In this paper, different circuit arrangements of Quantum-dot Cellular Automata (QCA) are proposed for the so-called coplanar crossing. These arrangements exploit the majority voting properties of QCA to allow a robust crossing of wires on the Cartesian plane. This is accomplished using enlarged lines and voting. Using a Bayesian Network (BN) based simulator, new results are provided to evaluate the robustness to so-called kink of these arrangements to thermal variations. The BN simulator provides fast and reliable computation of the signal polarization versus normalized temperature. It is shown that by modifying the layout, a higher polarization level can be achieved in the routed signal by utilizing the proposed QCA arrangements.*

## 1. Introduction

Quantum-dot Cellular Automata (QCA) [12] is a promising technology that could allow to overcome some of the limitations of current technologies, while meeting the density foreseen by Moore's Law and the International Technology Roadmap for Semiconductors (ITRS). For manufacturing, molecular QCA implementations have been proposed to allow for room temperature operation; the feature of wire crossing on the same plane (coplanar crossing) provides a significant advantage over CMOS. Coplanar crossing is very important for designing QCA circuits; multilayer QCA has been proposed [3] as an alternative technique to route signals, however it still lacks a physical implementation. At design level, algorithms have been proposed to reduce the number of coplanar wire crossings [8]. In QCA circuits, a reliable operation of coplanar crossing is dependent on the temperature of operation. Resilience to temperature variations due to thermal effects is also an important feature to consider. A reduction in the probability of generating an erroneous signal is also a concern, hence, robustness must be addressed.

Robustness to thermal effects must consider the repeated estimates of ground (and preferably near-ground) states, along with cell polarization for different design variations. This evaluation is presently possible only through a full quantum-mechanical simulation (over time) that is known to be computationally expensive. AQUINAS [12] and the coherence vector simulation engine of QCADesigner [13] perform an iterative quantum mechanical simulation (as a self consistent approximation, or SCA) by factorizing the joint wave function over all QCA cells into a product of individual cell wave functions (using the Hartree-Fock approximation). This results in accurate estimates of ground states, cell polarization (or probability of cell state), temporal progress and thermal effects, but at the expense of a large computational complexity. Other techniques such as QBert [9], Fountain-Excel simulation, nonlinear simulation [10, 13], and digital simulation [13] are fast, but they only estimate the state of the cells; in some cases unfortunately, they may fail to estimate the correct ground state. Also these techniques do not fully estimate the cell polarization or take into account thermal effects. In this paper, we use a modeling method that allows not only to estimate the cell polarization for the ground state, but to study the effects of thermal variations. Using a Bayesian model, it is possible to model and perform a thermal characterization of the coplanar crossing (which is not possible by iterative quantum mechanical simulation).

The objective of this paper is to propose and analyze different circuit arrangements for QCA coplanar crossing.

The co-planar crossing designs that we discuss are: (1) two normal coplanar crossings [7], (2)two TMR based coplanar crossing proposed by us in this work and (3)two thick coplanar crossing [2]. Even though we could study the effect of changing radius of effect, cell sizes, clock energy, in this work, we focus on the robust operation to thermal variation in detail assuming a conventional radius of effect of 2 neighboring cells. The proposed arrangements utilize the majority voting function of QCA circuits to route signals on a Cartesian plane. This feature is also made possible by the different types of cells (rotated and not rotated) and their immediate adjacencies.

This paper is organized as follows: Section 2 provides an overview of QCA technology, Section 3 introduces the Bayesian model used for temperature characterization and Section 4 describes the coplanar wire crossing arrangements (inclusive of layouts). Section 5 provides an analysis of the designs with respect to normalized temperature. Finally, Section 6 draws conclusions on the analysis.

## 2. Review of QCA

A QCA cell can be viewed as a set of four charge containers or "dots", positioned at the corners of a square. The cell contains two extra mobile electrons which can quantum mechanically tunnel between dots, but not cells. The electrons are forced to the corner positions by Coulomb repulsion.

Therefore electrons have a preferential alignment along one of the two perpendicular cell axes, as shown in Fig. 1. The polarization $\delta$ [1] measures the extent of this alignment. If the two extra electrons are completely localized on dots 1 and 3, the polarization is + 1 (binary 1); if they are localized on dots 2 and 4, the polarization is - 1 (binary 0). Tunneling between dots implies that charges may not be not completely localized and consequently the polarization value can be not integer.

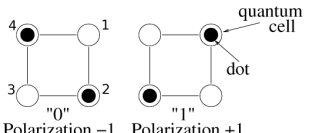


**Figure 1. QCA cell and polarization states**

Unlike conventional logic circuits in which information is transferred by electrical current, QCA operates by the Coulombic interaction that connects the state of one cell to the state of its neighbors. This results in a technology in which information transfer (interconnection) is the same as information transformation (logic manipulation) with low power dissipation [11].

1 $\delta$ refers to polarization as $P$ is used for defining probabilities.

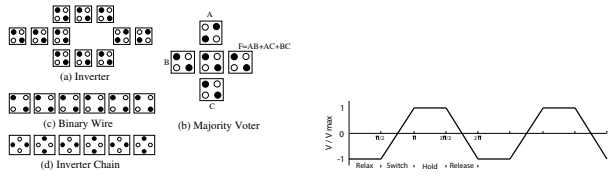


**Figure 2. (1) Basic QCA devices (2) Cmos-Clock-Signal**

One of the basic logic gates in QCA is the so-called majority voter (MV) with logic function Maj$(A, B, C) = AB + AC + BC$. MV can be realized by 5 QCA cells, as shown in Figure 2(1b). Logic AND and OR functions can be implemented from the MV by setting an input (the so-called programming or control input) permanently to a "0" or "1" value. The inverter (INV) is the other basic gate in QCA and is shown in Figure 2(1a). The binary wire and inverter chain (as interconnect fabric) are shown in Figure 2(1c)(1d). In VLSI systems, timing is controlled through a reference signal (i.e. the clock), however timing in QCA is accomplished by clocking in four distinct and periodic phases [4] (as shown in Figure 2 (2)). A QCA circuit is partitioned into *serial* (one-dimensional) zones, and each zone is maintained in a phase.

## 3. Bayesian Model

The two-state approximate model of a single QCA cell [12] is utilized. In this model, each cell can be observed to be in one of two possible states, corresponding to logical states 0 and 1. Let the probability of *observing* a QCA cell at state 0, be denoted by $P(X_i = 0)$ or $P_{X_i}(0)$, or simply by $P(x_i)$. Hence for *polarization*, $\delta_{X_i} = P_{X_i}(1) - P_{X_i}(0)$ The joint probability of observing a set of steady-state assignments for the cells is denoted by $P(x_1, \cdots, x_n)$. To reduce the combinatorial complexity of this analysis, the joint wave function must be considered in terms of the product of the wave function over one or two variables (i.e. the Slater determinants). This corresponds to a factored representation of the wave function (Hartree-Fock approximation)[11] [6]. As an example, consider the linear wire arrangement of 9 QCA cells, shown in Fig. 3(a). With no assumption, the joint state probability function can be decomposed into a product of *conditional* probability functions by the repeated use of the property that $P(A, B) = P(A|B)P(B)$ (as shown in Fig. 3d).

$$P(x_1, \cdots, x_9) = \\ = P(x_9|x_8 \cdots x_1)P(x_8|x_7 \cdots x_1) \cdots P(x_2|x_1)P(x_1) \quad (1)$$

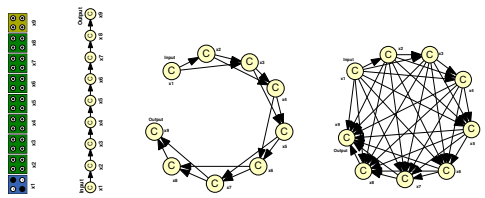

(a) (b) (c) (d)

**Figure 3. Bayesian net dependency model (BN) for (a) 9-cell QCA wire with (b) 1-cell radius of influence (c) 2-cell radius of influence, and (d) all cells.**

The radius of influence $r$ is the maximum distance (normalized to the cell-to-cell distance) that allows interaction between two cells. If a 2-cell radius ($r = 2$) of influence is considered, then the conditional probability $P(x_i|x_{i-1}, \cdots, x_1)$ can be approximated by $P(x_i|x_{i-1}, x_{i-2})$, and the overall joint probability can be factored as

$$P(x_1, \cdots, x_9) = \begin{cases} P(x_9|x_8, x_7)P(x_8|x_7, x_6) \cdots P(x_2|x_1)P(x_1) & r = 2 \\ P(x_9|x_8)P(x_8|x_7) \cdots P(x_2|x_1)P(x_1) & r = 1 \end{cases}$$

Hence, an inherent causal ordering is considered among cells (parent-child relationship) [1] as imposed by the clocking zones and the direction of propagation of the wave function [12] inside a single clocking zone. The conditional probabilities [1] $P(A|B)$ are then based on the condition that cells are always in the ground state; moreover, these probabilities are calculated from the diagonal entries of the steady-state density matrix $\rho_{00}\ and\ \rho_{11}$ which are given by:

$$\rho_{00}^{ss} = \frac{1}{2}\left(1 - \frac{E}{\Omega}\tanh(\Delta)\right) \quad (2)$$

$$\rho_{11}^{ss} = \frac{1}{2}\left(1 + \frac{E}{\Omega}\tanh(\Delta)\right) \quad (3)$$

where $E$ is the total kink energy at the cell, $\Omega = \sqrt{E^2 + \gamma^2}$ ($\gamma$ is the tunneling energy) is the energy term (also known as the Rabi frequency), and $\Delta = \frac{\Omega}{kT}$ is the thermal ratio $k$ is the Boltzmann's constant and $T$ is the temperature in Kelvin. Interested readers are encouraged to refer to [1] for a detailed treatment of this computational model.

## 4. Crossing Schemes

The coplanar wire crossing is one of the most interesting aspects of QCA; it allows for the physical intersection of horizontal and vertical QCA wires on the same plane while retaining logic independence in their values; the vertical wire is implemented by rotating the QCA-cells at 45 degrees i.e. by means of an inverter chain. The feature of this structure is that the information along the vertical wire does not interact with the horizontal, wire. Crossing is obtained by interrupting either the horizontal, or the vertical wire, these interruptions are hereafter also referred to as cuts. Switching of the signals is accomplished by the four phased clock through the release phase.

As in previous papers in the technical literature, layouts are considered to be in a single clocking zone. The outputs are evaluated when the ground state is attained by quasi adiabatic switching. A different approach [5] proposes the vertical and horizontal waves alternatively passing through an intersection. While this approach has the interesting feature of exploiting the intrinsically pipelined behavior of QCA, crossings in a single clocking zone require lesser area and a simple clocking circuitry.

Three novel schemes (and associated layouts) for coplanar crossing are introduced together with the corresponding BN.

1. *Normal crossing: this is based on the orientation of the cells.*
2. *TMR crossing: this is based on the voting nature in the QCA layout.*
3. *Thick crossing: this is based on the interaction among cells in an enlarged wire.*

For normal crossing the cell orientation is interrupted on the central cell of either the horizontal ($A$ line), or vertical line ($B$ line).

For the other two schemes, the cell orientation is interrupted on the horizontal ($A$ line), or vertical line ($B$ line).

### 4.1. Normal

The normal coplanar crossing arrangements (shown in Figs. 4 and 5) has been proposed in the technical literature [7]. It has been shown that an horizontal wire (with input $A$ and output $Aout$) can be crossed with a vertical inverter chain (with input $B$ and output $Bout$) with no interference among wires.

These arrangements differ by the orientation of the cell at the crossing point: $Xa$ in Fig. 4 (a) has the central cell rotated by 45 degrees, $Xb$ in Figs 5 (a) has a non-rotated cell. Figs 4 (b) and 5 (b) show the BN for analyzing these two arrangements. Note that only the BN shown in 4 (b) reports the actual number of connections which account for a radius of effect equal two, all the successive BNs are simplified for improving their readability.

### 4.2. TMR

A simple approach for implementing robust crossing in QCA is to take advantage of the inherent voting characteristic of this technology. The QCA wire is split through fanout, crossed and then re-converged and voted by a MV which performs a TMR voting function of the signals.

Two types of arrangements are proposed:

1. 3-to-1 TMR;

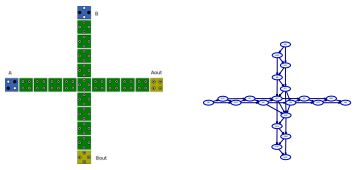

(a) (b)

**Figure 4. Normal crossing with rotated central cell ($Xa$) (a) Layout (b) BN with 2-cell radius of effect.**

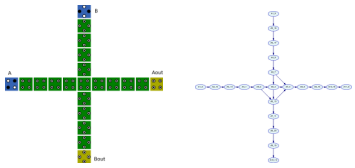

(a) (b)

**Figure 5. Normal crossing with rotated central cell ($Xb$) (a) Layout (b) BN with 2-cell radius of effect.**

2. 3-to-3 TMR.

In the 3-to-1 TMR architecture shown in Fig.6 and associated BN, voting occurs along the direction on which the cell rotation is interrupted, thus producing two different arrangements TMR_Xa for voting the $A$ line and TMR_Xb for voting the $B$ line (shown in Fig. 6 ) .

If both wires are split and reconverged, the more complex 3-to-3 (triple) TMR architecture (as shown in Fig. 7 with corresponding BN) is applicable. The triple TMR has also two versions: double_TMR Xa (Fig. 7) for the interrupted $A$ line direction, and double_TMR Xb for the interrupted $B$ line direction. The 3-to-3 TMR utilizes a larger number of cells (92 versus 41) than the 3-to-1 TMR.

### 4.3. Thick

A crossing arrangement that is still based on TMR voting, has been proposed in [2] and is hereafter referred to as thick crossing. Differently from TMR, in thick crossing the

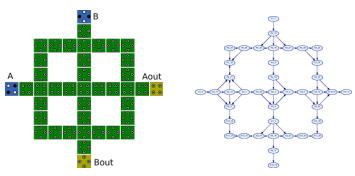


(a) (b)

**Figure 6. 3x1 TMR crossing with non rotated central cell (TMRXb voting on the B line) (a) Layout (b) BN with 2-cell radius of effect.**

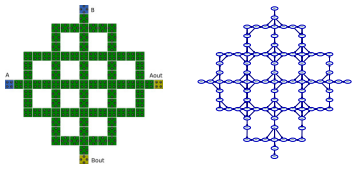

(a) (b)

**Figure 7. 3 x 3 TMR crossing with rotated central cell (a) Layout (b) BN with 2-cell radius of effect.**

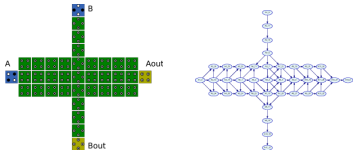


(a) (b)

**Figure 8. Thick horizontal crossing (a) Layout (b) BN with 2-cell radius of effect.**

fanout of the three wires generates a "thick" wire which has a width of three cells; crossing between wires is performed by interrupting the thick wire with a single wire whose cells are rotated with respect to the thick wire. Figs. 8 and 9 show these arrangements together with the corresponding BN for horizontal and vertical crossings. A thick organization requires 37 QCA cells.

## 5. Temperature Characterization

In this section, the simulation results are presented for the Bayesian network of the proposed coplanar crossing designs with respect to temperature. In all reported plots, starting from the correct value, the output value tends to 0 when the normalized temperature tends to one, i.e. when the temperature is such that $kT \simeq E_k$ (the thermal energy is equal to the kink energy) and the two extra electrons are delocalized. The increase in temperature has different effect on the layouts, therefore allowing to define a metric. Figs. 11, 12, 13 and 14 provide the plots of output value dependence on temperature for the previously introduced arrangements

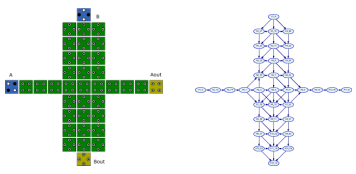

(a) (b)

**Figure 9. Thick vertical crossing (a) Layout (b) BN with 2-cell radius of effect.**

when considering the exhaustive four values of the $A, B$ inputs $i.e.$ $(0,0)$ $(1,0)$ $(0,1)$ and $(1,1)$ respectively. The plots show the robustness of the proposed designs with respect to a temperature increase: a steep slope at the output to reach the zero polarization accounts for an inefficient temperature solution, while a smooth slope shows a good temperature performance. A quantitative metric for evaluating the performance of the different arrangements is introduced by taking into account the increase of normalized temperature needed for dropping the output polarization from 90 % to 10% of the nominal value. This metric is referred to as Thermal robustness ($Th$) and is defined as

$$Th = \Delta T_{\Delta P_{90-10}}$$

Tables 1 and 2 report the $Th$ computed for $Aout$ and $Bout$ respectively for the considered coplanar crossing schemes the higher values account for better performances.

The following observation can be drawn from analyzing the plots and tables :

1) In all configurations, thermal robustness is not affected by input values, $i.e.$ there is no correlation between polarization levels for boolean states and temperature;

2) In all configurations, the outputs along the non interrupted direction behave similarly: for instance in the $A$ direction ThickXb, Xb and TMRXb result in the same $Th$ because there is no interrupted wire in such direction

3) The double TMR layout always has the worst performance on the interrupted direction $i.e.$ dblTMRXa has the worst $Th$ value in Table 1 while dblTMRXb has the worst $Th$ value in Table 2.

4) Thick crossings have always the best performance on the interrupted direction

5) The number of cuts reduces performance, for instance double TMRXa has worse performance than TMR Xa.

In general, the $Th$ of $Bout$ is higher than $Aout$ for the same design. This is also applicable if "uncut" arrangements are compared in the designs. For example, in Table 1, $Aout$ for Xb is 0.383, while in Table 2 $Bout$ for Xa is 0.543.

The last observation can be explained as follows. The kink energy between two cells is determined by the difference in energy between the higher energy configuration and the lower energy configuration. Assuming two possible states for each cell, we can have two possible energy configurations of 2 cells as shown in Fig. 10.

The energy of each configuration is computed by summing the Coulomb energies between the dots in the cells:

$$E_{12} = \sum_{i=1}^{4} \sum_{j=1}^{4} \frac{q_{1i} q_{2i}}{4\pi\epsilon\epsilon_r} \frac{1}{d_{ij}} \tag{4}$$

The charge at the $i-th$ dot of the first cell is denoted by $q1i$, and the distance between the $i-th$ dot in the first cell and the $j-th$ dot in the second cell is denoted by $d_{ij}$. On the assumption that there exists an effective $-1/2q$ charge

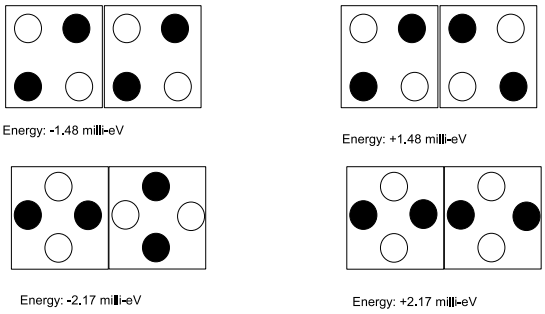


**Figure 10. Configuration energies for normal (top row) and rotated (bottom row) cells. (left the lowest energy configurations, right the highest energy configurations)**

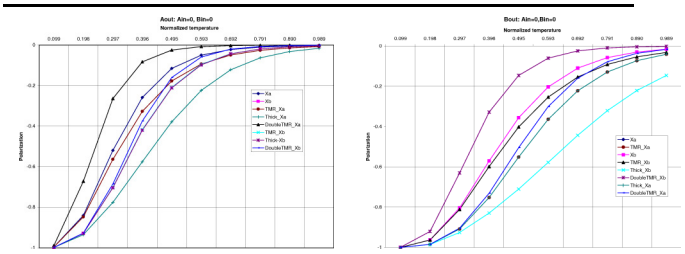

(a) (b)

**Figure 11. Output polarization vs normalized temperature for A=0 B=0 (a) Aout(b) Bout**

at each black dot and $+1/2q$ at the white dots, the overall charge of a cell is zero. The kink energy for the normal cell is 2.96 milli eV, while the energy of the rotated cell is higher at 4.34 milli eV. The difference in kink energy is due to the difference in distance between the dots for the cell types. The largest distance between two dots occurs for the normal cells than for rotated cells. Therefore, this suggests that a rotated cell arrangement is thermally more stable than a non-rotated one.

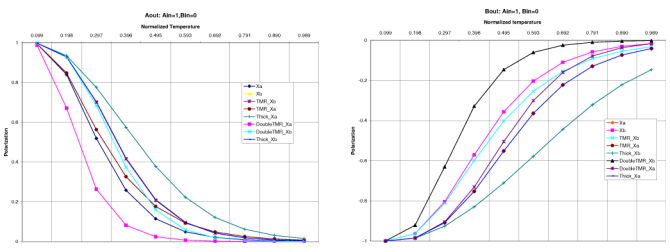

(a) (b)

**Figure 12. Output polarization vs normalized temperature for A=1 B=0 (a) Aout(b) Bout**

| A | B | Xa | Xb | TMRXa | TMRXb | dblTMRXa | dblTMRXb | ThickXa | ThickXb | Average |
|---|---|---|---|---|---|---|---|---|---|---|
| 0 | 0 | 0.355 | 0.383 | 0.429 | 0.383 | 0.263 | 0.35 | 0.457 | 0.383 | 0.375375 |
| 0 | 1 | 0.355 | 0.383 | 0.429 | 0.383 | 0.263 | 0.35 | 0.457 | 0.383 | 0.375375 |
| 1 | 0 | 0.355 | 0.383 | 0.429 | 0.383 | 0.263 | 0.35 | 0.457 | 0.383 | 0.375375 |
| 1 | 1 | 0.355 | 0.383 | 0.429 | 0.383 | 0.263 | 0.35 | 0.457 | 0.383 | 0.375375 |

| A | B | Xa | Xb | TMRXa | TMRXb | dblTMRXa | dblTMRXb | ThickXa | ThickXb | Average |
|---|---|---|---|---|---|---|---|---|---|---|
| 0 | 0 | 0.543 | 0.474 | 0.543 | 0.54 | 0.46 | 0.33 | 0.543 | 0.679 | 0.514 |
| 0 | 1 | 0.543 | 0.474 | 0.543 | 0.54 | 0.46 | 0.33 | 0.543 | 0.679 | 0.514 |
| 1 | 0 | 0.543 | 0.474 | 0.543 | 0.54 | 0.46 | 0.33 | 0.543 | 0.679 | 0.514 |
| 1 | 1 | 0.543 | 0.474 | 0.543 | 0.54 | 0.46 | 0.33 | 0.543 | 0.679 | 0.514 |

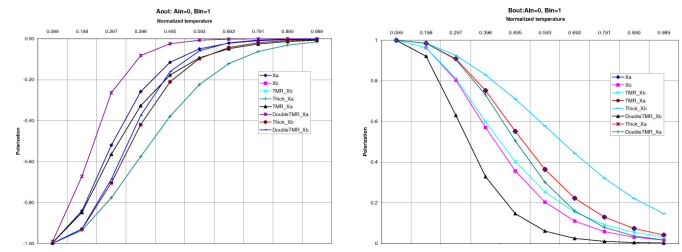

(a) (b)

**Figure 13. Output polarization vs normalized temperature for A=0 B=1 (a) Aout(b) Bout**

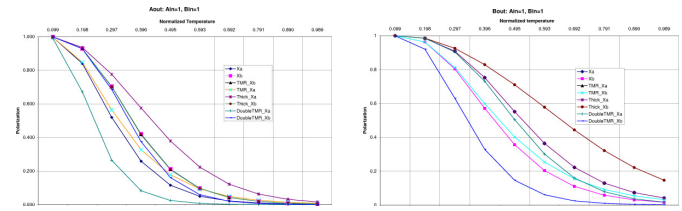

(a) (b)

**Figure 14. Output polarization vs normalized temperature for A=1 B=1 (a) Aout(b) Bout**

## 6. Conclusion

This paper has provided the analysis of the thermal properties of different designs for implementing the robust coplanar crossing for Quantum-dot Cellular Automata (QCA) based circuits. The use of a Bayesian Network BN simulator has allowed for fast and reliable computation to evaluate the thermal performance of different layouts. It has been shown that, in all configurations, thermal robustness is not affected by input values, and the use of the so-called thick crossing scheme accounts for the best resilience to temperature. Moreover, from the simulation results it has been noticed and then proved that wires with rotated cells are thermally more stable than a non-rotated scheme. Future work include the investigation of the coplanar crossing structures in presence of cells placement defects and variations of clock energy and radius of effect.

## References


[1] S. Bhanja, S.; Sarkar. Graphical probabilistic inference for ground state and near-ground state computing in qca circuits. In *IEEE Conference on Nanotechnology*, July 2005.

[2] A. Fijany, N. Toomarian, and K. Modarress. Block qca fault-tolerant logic gates. Technical report, Jet Propulsion Laboratory, California, 2003.

[3] A. Gin, P. D. Tougaw, and S. Williams. An alternative geometry for quantum-dot cellular automata. *J. Appl. Phys.*, 85(12):8281–8286, June 1999.

[4] K. Hennessy and C. Lent. Clocking of molecular quantum-dot cellular automata. *Journal of Vacuum Science and Technology*, 19(B):1752–1755, 2001.

[5] C. Lent. Molecular quantum-dot cellular automata. *Seminar*, May 2004.

[6] C. Lent and P. Tougaw. Lines of interacting quantum-dot cells - a binary wire. *Journal of Applied Physics*, 74:6227–6233, 1993.

[7] C. Lent and P. Tougaw. A device architecture for computing with quantum dots. *Proceedings of the IEEE*, 85(4):541–557, April 1997.

[8] S. K. Lim, R. Ravichandran, and M. Niemier. Partitioning and placement for buildable qca circuits. *J. Emerg. Technol. Comput. Syst.*, 1(1):50–72, 2005.

[9] P. M. Niemier, M.T.; Kontz M.J.; Kogge. A design of and design tools for a novel quantum dot based microprocessor. In *Design Automation Conference*, pages 227–232, June 2000.

[10] G. Toth. *Correlation and Coherence in Quantum-dot Cellular Automata*. PhD thesis, University of Notre Dame, 2000.

[11] P. D. Tougaw and C. S. Lent. Logical devices implemented using quantum cellular automata. *Journal of Applied Physics*, 75(3):1818–1825, Oct 1994.

[12] P. D. Tougaw and C. S. Lent. Dynamic behavior of quantum cellular automata. *Journal of Applied Physics*, 80(15):4722–4736, Oct 1996.

[13] K. Walus, T. Dysart, G. Jullien, and R. Budiman. QCADesigner: A rapid design and simulation tool for quantum-dot cellular automata. *IEEE Trans. on Nanotechnology*, 3(1):26–29, 2004.